HSM02 Magnet Fabrication and Test Summary

N. Andreev, G. Chlachidze, V. S. Kashikhin, M. J. Lamm, A. Makarov, M. Tartaglia, M. Yu

I. Introduction

The Fermilab magnet systems department is developing a series of helical solenoid magnets to demonstrate, in stages, the technology for muon cooling in a helical cooling channel [1-6]. The first prototype magnet, HSM01, was fabricated and tested in 2009 [7]. The design of HSM02 was very similar to HSM01, with four offset coils wound from SSC NbTi cable with continuous transition (no splices) between coil layers. A number of improvements were made based upon the HSM01 results, notably improved insulation and epoxy impregnation schemes, alignment features, and containing 10 turns of cable (versus 37 turns total in HSM01) in each coil. The HSM02 magnet fabrication was completed in June 2010. The magnet was tested in the Vertical Magnet Test Facility (VMTF) with the first cold test beginning in November 2010, followed by a conduction cooling study and second cold test cycle in December. The fabrication details and test results are presented here.

II. Fabrication

The HSM02 design parameters are given in Table 1. A cross sectional view of the magnet with as-built dimensions is shown in Figure II-1. The design of the HSM02 was slightly revised from the HSM01 in order to eliminate some problems noticed at the HSM01 fabrication and tests:

- The cable was re-sized to minimize the key-stoning effect. Subsequent short sample tests were performed, which demonstrated there was no degradation of the critical current after cable was flattened.
- The inner and outer rings height was increased from 20 mm to 23.5 mm to ensure 10 turns fit in each layer (1 layer has 10 turns and 3 layers have only 9 turns in the HSM01).
- The locking steps/grooves were eliminated between 1-th layer rings and bottom flange (replaced with dowel pins), and between 4-th layer rings and upper flange (no pins).
- The G-10 rings covering the coil from both top and bottom in each layer were made wider to eliminate the possibility of coil to ground shorts in the cable transition areas between layers.
- The strip heaters were placed on the inner rings O.D. prior to winding (this provides more predictable and better contact between coil and heaters, and easier to install heaters).
- The HSM02 is furnished with copper cooling tubes, installed in special slots on the outer rings O.D. to check the efficiency of external conduction cooling in this solenoid design.
- Additional holes for the alignment balls made in the bottom flange before the winding allows tying up accurately the measured field configuration with the coil orientation.
- The coil leads insulators were made slightly different to eliminate the possibility of coil to ground shorts in these areas.
- The coil was impregnated in two steps: the first step – with plain epoxy, the second step – with the same epoxy, additionally mixed with mica powder. The mica powder filled epoxy is intended to displace the plain epoxy in the coil big voids to prevent epoxy cracking in these areas (which happened in the HSM01).

Table 1: Solenoid Parameters

Parameter	Units	Value
Coil inner diameter	mm	426
Coil outer diameter	mm	455
NbTi superconducting cable	mm	12.34 x 1.46
Cable critical current at 7 T, 4.2 K	A	9660
J_c (non-Cu)	A/mm^2	1730
Copper to superconductor ratio		1.5:1
Strand diameter	mm	0.8
Helical orbit radius	mm	255
Number of turns per coil		10
Coil width	mm	20

d_i (mm)	426.5
w (mm)	13.5
t (mm)	1.8
a (mm)	23.5
b (mm)	30
No. turns (turns/coil)	10
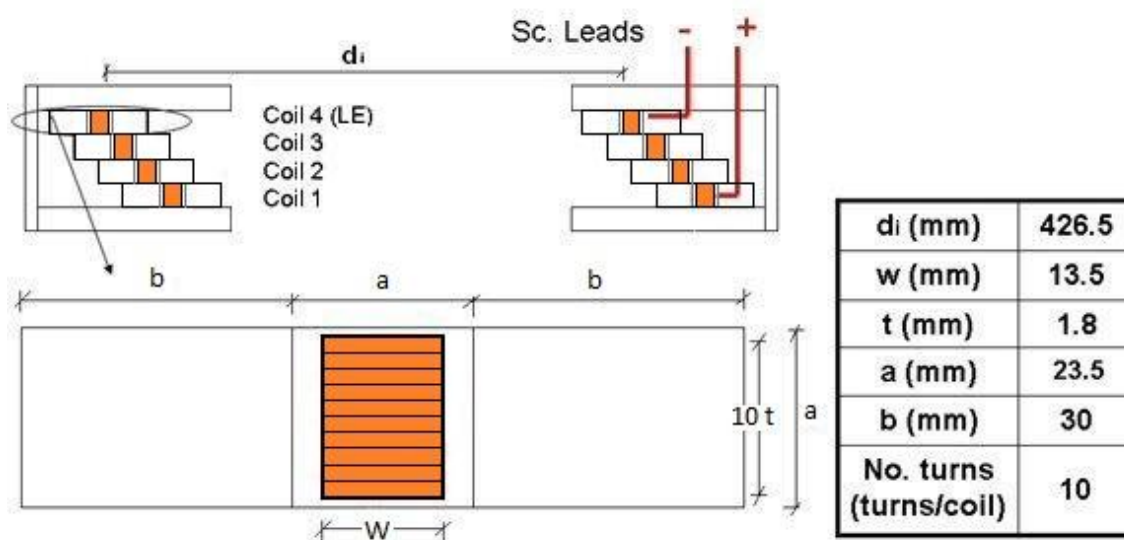
Fig. II-1. HSM02 structure, coil cross sections, and dimensions

The assembly was fabricated as follows: A bobbin with the pre-insulated cable was installed on the tensioner. All outer rings were clamped to a support, installed between tensioner and winding table. The cable lead from the tensioner was routed through all outer rings allowing their further assembly with the inner rings. The lead was secured in the G-10 lead insulator, installed in the bottom flange. The heaters were glued to the inner rings O.D. prior to coil winding with heaters leads routed inside the solenoid through the slots provided in the inner rings. Three voltage taps soldered to the coil at the layer-to-layer transitions also were routed inside the solenoid through the slots in the inner rings. Since the coil cable was wound hard way, each turn was clamped down with a special fixture to prevent the cable from popping out during the winding. This fixture was fixed on the inner ring, and had to be removed once all 10 turns of each layer wound in order to allow the outer ring and next layer inner ring installation. To prevent the cable from popping out once the fixture removed from solenoid, all turns were glued to each

other in the fixture clamps location (8 spots equally spaced on the diameter). The inner rings are tack welded to each other and to the bottom flange. This is critical for using of this clamp down fixture, and also allows locking the rings in the right location. The outer rings are tack welded to each other for the proper rings location locking only.

Once all four layers of the solenoid coil were wound, the top flange was installed and lined up with the bottom flange using the outer skin. The coil leads were insulated from both flanges, solenoid was compressed in the axial direction, and electrically tested (1 kV hipot of coil to ground, coil to heaters, and heaters to ground; ring test at 100 V, 100 Hz; Ls and Q measured at 100 Hz and 1 kHz; coil resistance and each heater resistance measured at room temperature). Then the top flange was tack welded to the upper inner ring, and the skin was removed for the cooling tube installation. The whole electrical test was repeated frequently during the solenoid fabrication (after each welding completed, prior to potting, after the potting, and at the skin welding, and at final inspection). The electrical test report can be found at the following website: http://tiweb.fnal.gov/MSDelog/controller/Entry?id=28022.
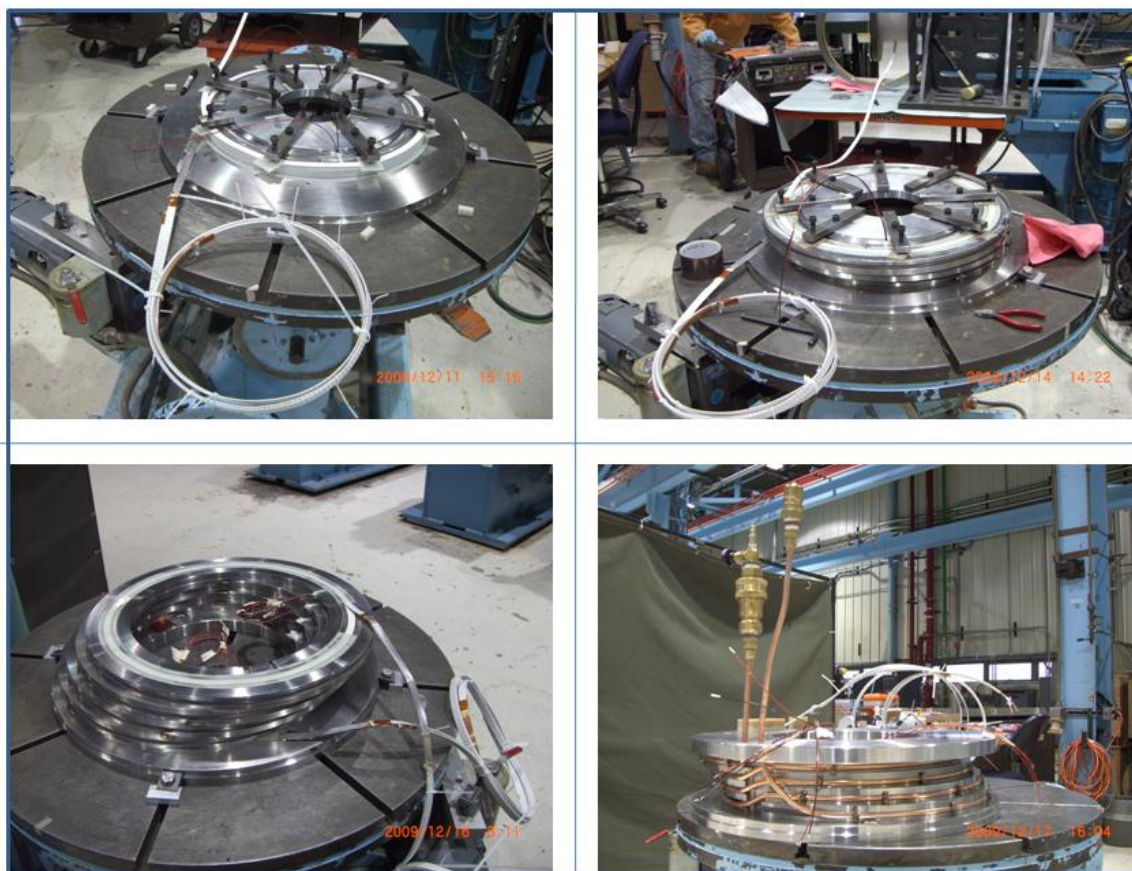

Fig. II-2. HSM02 Fabrication photos.

III. Test Overview

Voltages across each coil were monitored with one voltage tap segment per coil, from the SC lead to the transition regions for the outer coils, and from transition to transition for the inner two coils. Voltage for each coil was separately recorded in both Fixed Voltage Taps (FVT) and Configurable Voltage Taps (CVT, which have a wider range of gain selection options, allowing better signal

resolution); note that the FVT quadrant Q1 signal did not work. Coils were sequentially labeled A, B, C, D, with A the top (negative lead) and D the bottom (positive lead) coil. However, due to a mistake in configuring the logger readout signals, the voltage segment names are reversed – as discussed again later. The "half coil" segments for quench protection were made up of segments H1=A+B and H2=C+D. Unlike HSM01, the HSM02 magnet did not suffer any problems with ground insulation, and passed 1000 V hipots under both warm and cold conditions.

The temperature and strain gauge sensors are shown in Fig. III-1. A Cernox temperature sensor was attached to the inner circumference of each ring, as well as the inner circumference of the top and bottom support plates, to measure temperatures of the coil rings during the test. A strain gauge was mounted on the inner surface of the bobbin for each coil; a compensator strain gauge was also mounted on a tab welded to one coil ring.

As discussed in section II, a stainless steel strip heater was installed between the coil and inner ring of each layer. Thus four separate strip heaters were available for studies of their effectiveness at initiating quenches. Each heater had a warm resistance of about 0.45 Ohm, and cold resistance of 0.2 Ohm; thus an external resistor of 4 Ohms was put in series to allow greater range of adjustment in the deposited energy with the available heater firing units.

The Magnet Description document, which captures the salient attributes, instrumentation and test plan for the magnet, is posted at http://tiweb.fnal.gov/website/controller/1827. The magnet was mounted to the 30 kA Top Plate assembly for VMTF and final preparations for testing were completed the first week of November 2010. Fig. III-2 shows the magnet connected to the assembly prior to installation into the dewar. This figure gives the relative orientation of features (SC leads, N2 cooling tubes), which helps define the orientation and coordinate system for cold magnetic measurements. The lack of a flux return yoke and resulting large fringe fields required careful support of the superconducting (SC) leads to prevent motion-induced quenches (in fact, none occurred).
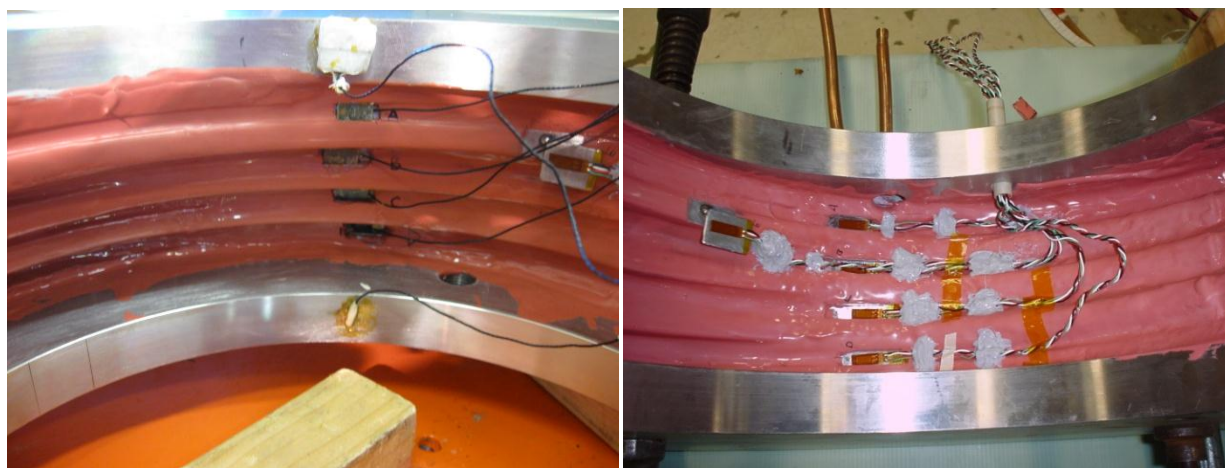

Fig. III-1. Cernox RTDs being mounted on HSM02 coil inner rings and support plates (left) and Strain gauges located on HSM02 coil inner rings, and compensator gauge on welded tab (right).

The magnet was tested in a pool boiling helium bath at the Vertical Magnet Test Facility (VMTF) in two cold test cycles, with an intervening "conduction cooling study" (discussed in detail later). The first cool down to 4.6 K occurred on November 06. The magnet passed cold ground insulation hipot test of 1000 V with leakage current 0.5 µA on 11/09, followed by a heater-induced quench at 1000 A to check

the quench protection system. Quench training and ramp rate dependence studies at 4.5 K began on 11/10; quench training at 3.0 K was performed from 11/15 until 11/17, and was followed by additional quench studies at 4.5 K. A thermal margin study was made on 10/14. Training and ramp rate studies continued until October 15 at which time the MTF cryogenic plant was shut down for maintenance (corresponding with the TD maintenance power outage on 10/16) until 10/26. Cold RRR data were obtained on 11/22, while warm data were taken on 11/05 (before cool down). **During the RRR measurement, it was realized from the timing of the resistive coil transitions and the temperature profile, that the RTD positions are correct (A=top, D=bottom), but the coil voltage tap segment** *names* **were reversed** (A=bottom, D=top; this was due to an incorrect assumption that the positive lead connected to coil A). Based upon the warm resistance values, the strain gauge identities are thought to be correct (A=top, D=bottom). Note also that the quadrant labels (Q1-Q4) are correct and are the same as HSM01: Q1=D(4)=LE, Q3=C(3), Q4=B(2), Q2=A(1)=RE.

Fig. III-2. HSM02 mounted to the 30 kA Top Plate Assembly prior to insertion into VMTF.

The LN2 conduction cooling study began at room temperature on 11/30 and continued through 12/01 as the temperatures reached equilibrium near 92 K. The assembly was again warmed to 285 K, and the second cool down to 4.6 K took place on 12/3. Quench re-training studies continued until 12/09, after which HSM02 was warmed up to room temperature. The magnet was removed from VMTF on 1/3, and a final electrical checkout was performed on 1/4.

IV. Cold Magnetic Field Measurements

A 3-axis Senis Hall probe (S/N 26-05) with 10 T range was used to capture the axial magnetic field strength profile with the magnet powered at 5000 A. This allows comparison to the magnetic field model prediction for the field at the solenoid "center", to validate the model (which is used to predict the peak field on the coils, and quench current). The prediction was made using Opera3D, constructed using the as-built geometry (defined by drawing #467121). The Hall probe was mounted on a long G-10 shaft within a probe support and bearings that centered it, with B_z aligned with the magnet axis. A scale on the shaft allowed manual positioning with <1 mm accuracy. Angular orientation of the probe was possible by aligning the shaft scale to marks on the warm bore flange, so the B_x and B_y values were also studied. Fig. IV-1 shows the Hall probe and HSM02 coordinate system. A comparison of measured and predicted B_z versus Z-Z_0, where the center point Z_0 is obtained from the measured B_z symmetry, is given in Fig. IV-2.
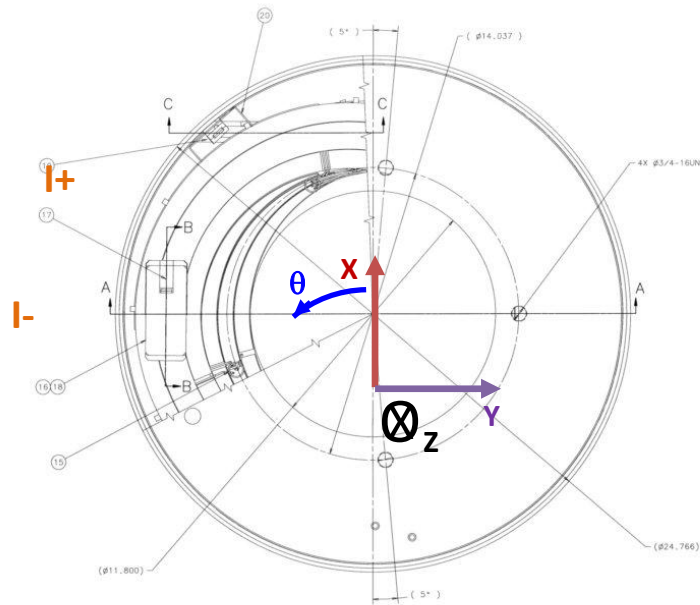
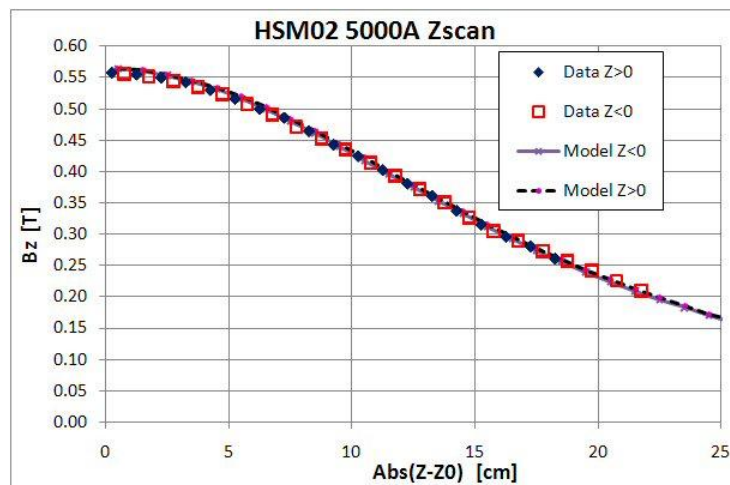Fig. IV-1. 3D Hall Probe Coordinate System at VMTF viewed from Top of HSM02 (drawing 467121).

Fig. IV-2. Measured and predicted axial field strength (B_z) versus position along the solenoid axis (Z).

At the position Z_0 of B_z symmetry, two additional measurements were taken: first, the transverse components B_x and B_y were measured as a function of angle at 5000 A. Second, all three components were measured as a function of the magnet current, up to 12000 A, to gauge linearity of the field. Fig. IV-3 shows the angle dependence of B_x, B_y, and B_z, with sinusoidal fits superimposed; error bars reflect the rms scatter for 10 measurements taken at each Z position, $\sim 3/\sqrt{(10)}$ G. The fits are made to the function **B(θ) = a · sin((b·θ + c) + d** with **b** constrained to be 1; fit parameters are listed in Table 1. The Opera3D model prediction is shown in Fig. 7, and expectations are also included in Table 1.
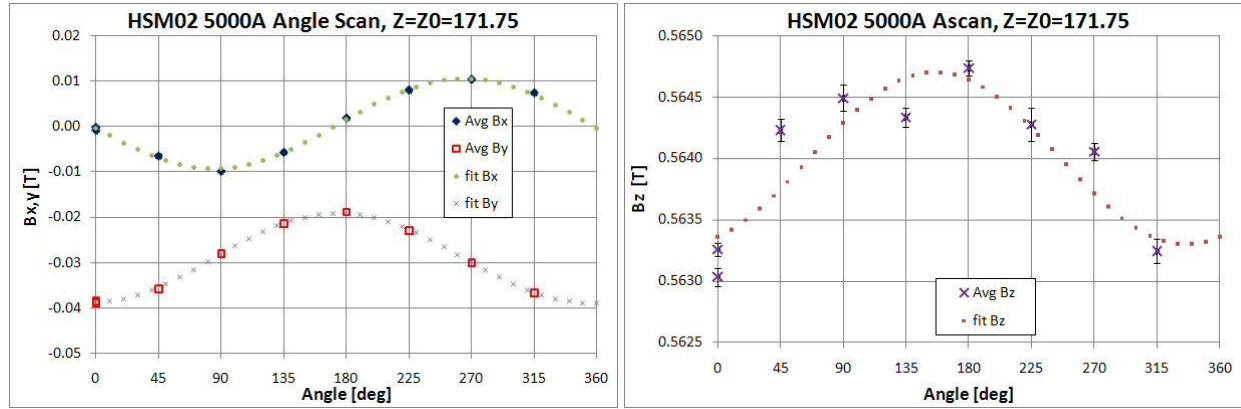
Fig. IV-3. Angle dependence of x,y (left) and z (right) field components at Z_0, at 5000 A.
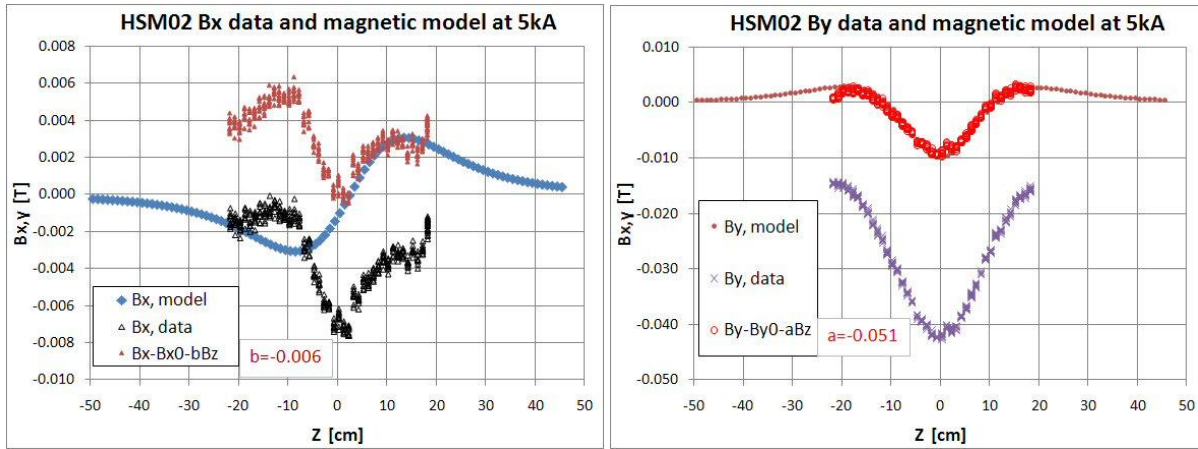
Fig. IV-4. Predicted and measured transverse field components (in Hall probe coordinate system) as a function of $Z-Z_0$.

Table 1. Parameters of sinusoidal fits and predictions for angle dependence of field components

Field component	**a**, strength [T]	**a**, predicted	**c**, phase [deg]	**d**, offset [deg]	**d**, predicted
B_x	-0.0099	-0.0099	5.2	-0.0007	0
B_y	-0.0099	-0.0099	95.3	-0.0290	0
B_z	-0.0007	0	114.1	0.5640	.5644

The Opera3D model prediction at the Z_0 position is in good absolute agreement with the measurements: the transverse field is dominated by B_y, and both B_x and B_y should have the same

amplitude with a phase difference of 90 degrees, as we see. The offset in both X and Y directions should be zero. That B_y has a rather large offset can easily be explained if there is a slight tilt α of the probe in the Y-Z plane, which introduces a projection of B_z onto the Y axis; thus $D_y = B_z \cdot \sin(\alpha) \approx B_z \cdot \alpha$, so $\alpha =$ .029/.564 = 0.051 radians $\approx$ 3 degrees. Such a tilt is certainly possible, since we found after removing the probe that the ceramic reference plate, which aligns the probe in its G10 holder, has separated from the probe and was lost. In Fig. IV-4, the measured Z-dependence of B_x and B_y are shown with the model; subtracting a B_z term with coefficient 0.058 shows a reasonable agreement with the model B_y; B_x is not as good, but given that we do not know the precise probe location within the magnet, this is not really a concern. Warm measurements will provide a better comparison with the model.

Fringe field measurements were made at the VMTF floor level, which was 2.4 m above the magnet center. These are important because lack of a return yoke results in an extended fringe field that poses a safety concern. The measurements were made using a Walker, Inc. hand-held Hall probe (bar code 835) and Gauss meter (bar code 834) that had been zeroed away from sources of magnetic field. Fig. IV-5 shows the measured field magnitude (B_{mod}) versus distance going north from the warm bore tube, taken at floor level at 9000 A (the maximum current reached was $\approx$15000 A). The 5 Gauss pacemaker limit is about 2 meters from the warm bore at floor level.
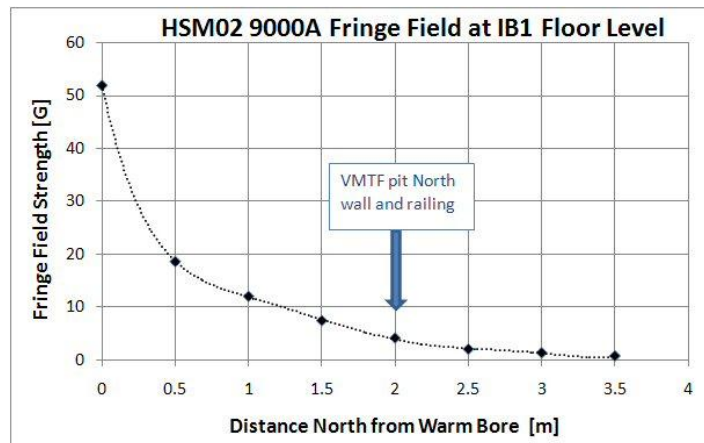

Fig. IV-5. Fringe Field magnitude versus radial distance from the magnet axis, at floor level at 9000 A.

V. Warm Magnetic Field Measurements

The test stand B used for Hall probe point scan field mapping of HSM01 was unavailable for mapping HSM02, due to high priority accelerator support demands. Therefore an alternative, new system was utilized after completion of the cold testing. The new system was assembled and LabView motion control and readout software were developed during the summer of 2011. Fig. V-1 shows the arrangement of motion stages: Y (vertical) and Z (axial) motions are automated, while the X (transverse) motion is done with a precision indexed manual stage. The solenoid and stages are mounted above a steel girder, with the solenoid base raised 12" above the table using an aluminum box beam. A new 2 T, 0.1% linearity calibrated 3D Senis Hall probe (S/N58-11) was installed in an aluminum probe holder which was mounted to the end of a long aluminum beam supported by the vertical stage. The probe and motion control system have the same coordinate system: Y is positive up, X is positive to the North, and Z is positive to the East (from non-Lead towards Lead end). The HSM02 non-lead end has machined holes for installation of survey fiducials. The solenoid orientation was shimmed to make the non-lead end

surface vertical, and adjusted to make the same surface normal to the edge of the steel table. The probe motion system was also adjusted so that the motion along Z was parallel to the table edge, X perpendicular to that edge, and Y vertical. Errors in the motion are estimated to be up to 10 milliradians in each direction; at this time, a survey of the magnet and probe to determine the relative coordinates of each coil ring and the probe is anticipated but has not yet been performed. When the system is positioned at "Z=0", the Hall probe active element is 196 mm from the RE plate surface in the negative Z direction. For warm magnetic measurements a central axis X=0, Y=0 is defined to be the center of the RE plate aperture (which coincides with the LE aperture).

Data were taken by positioning the probe to specific {X,Y} points, then scanning in Z from Z=0 to ~540 mm in 10 mm steps. Ten measurements were taken at each Z position. Each scan was made at both +10 A and -10 A in quick succession (which were then "averaged"). Several measurements were repeated a number of times, and some zero current scans were taken at two X,Y positions with 100 points per z step, to study noise and drift of the Hall probe voltage signals (as well as investigate some possible small anomalies due to welds on the coil inner rings). The main data sets consist of Z scans at the following points, {X,Y} = {0, 0}, {0, -100 mm}, {0, 100 mm}, {-4.0 in, 0}, {4.0", 0}. These data are located in:
S:\Run Support\VMTF\LIST_of_MAGNETS\MuCool_HSM02\MagneticMeasurements\WarmMagMeas\ScanSummaries
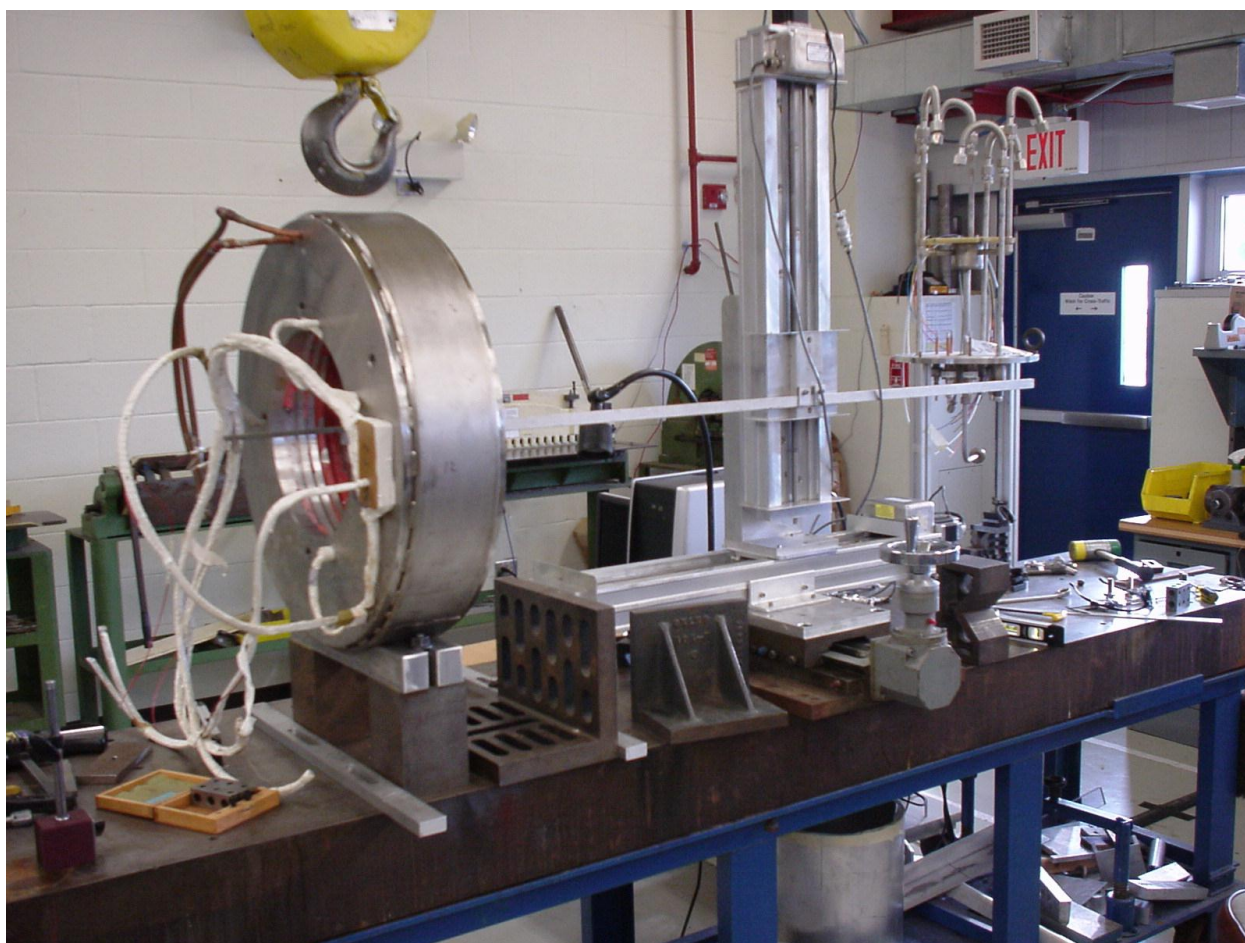

Fig. V-1. View of overall scan system setup (before probe support shaft length adjustment, SC lead arrangement, and removal of magnetic materials used to adjust alignment).
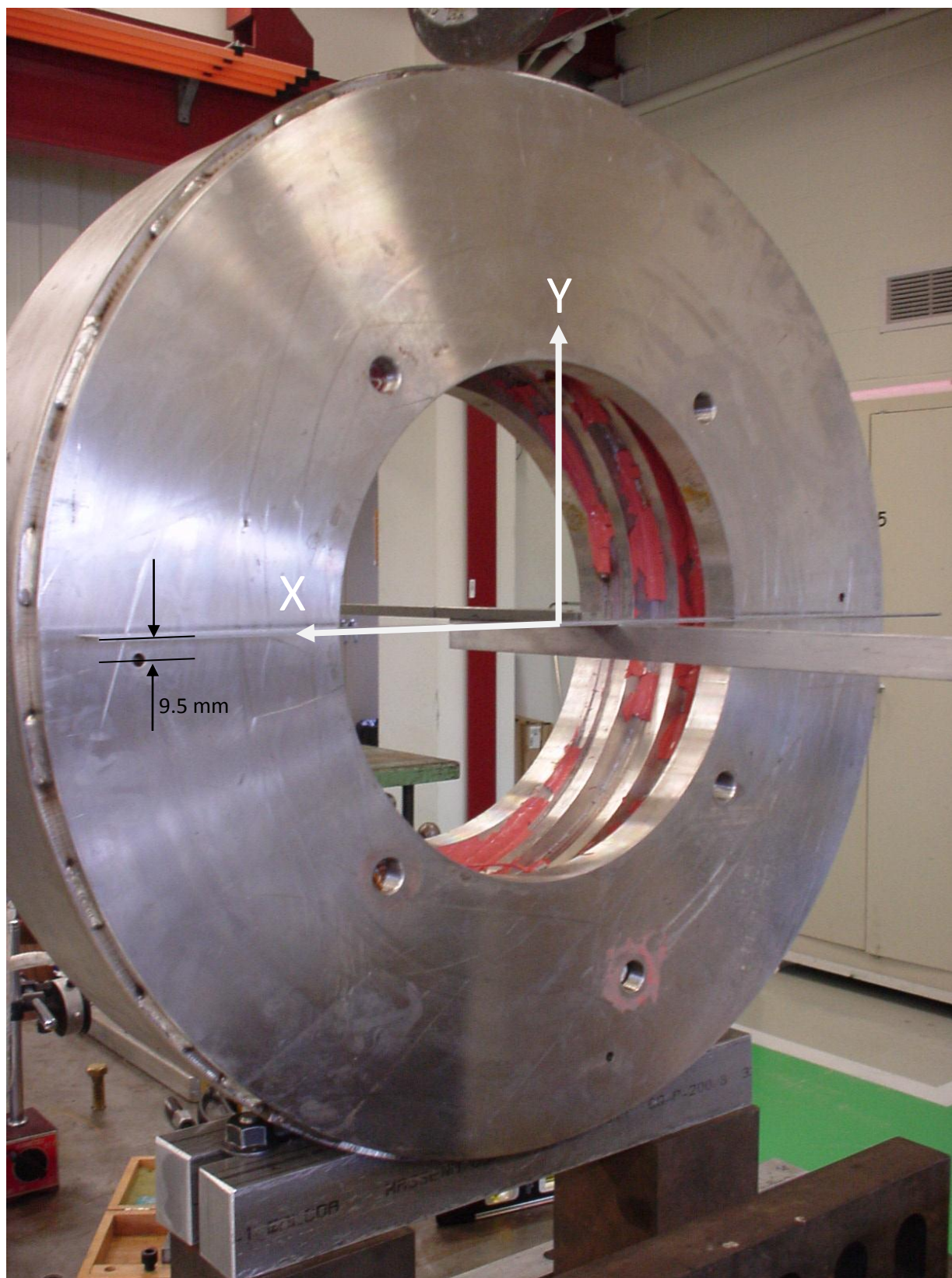
Fig. V-2. Non-lead side of the HSM02 solenoid, probe motion coordinate system and survey target holes.
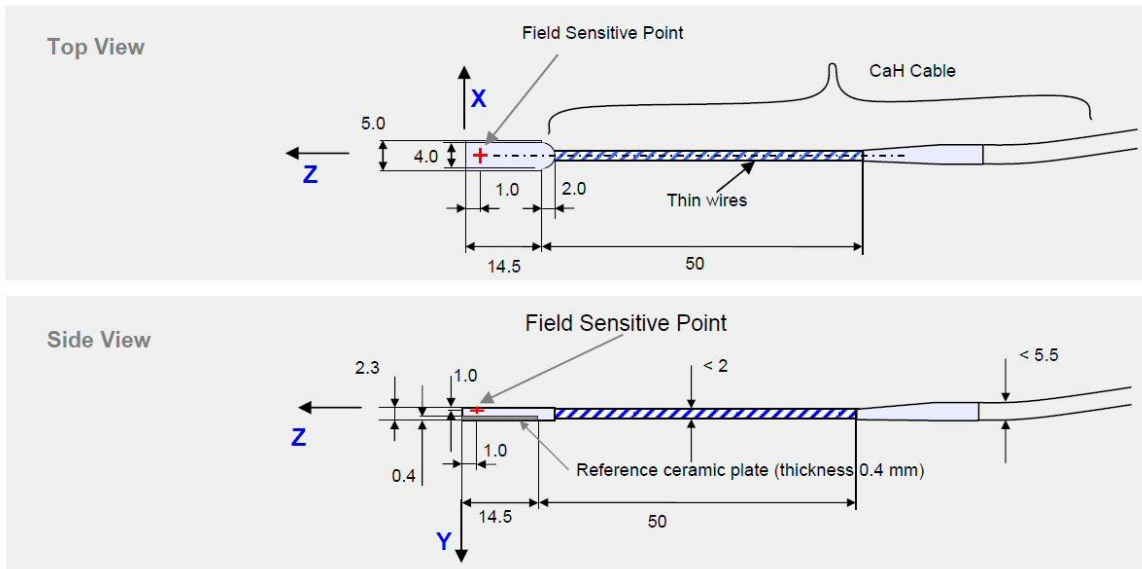
Figure 1:   Dimensions of the SENIS C-H3A-xx Hall probe (all measures are shown in mm). Field sensitive point (FSP) is marked with a red cross.
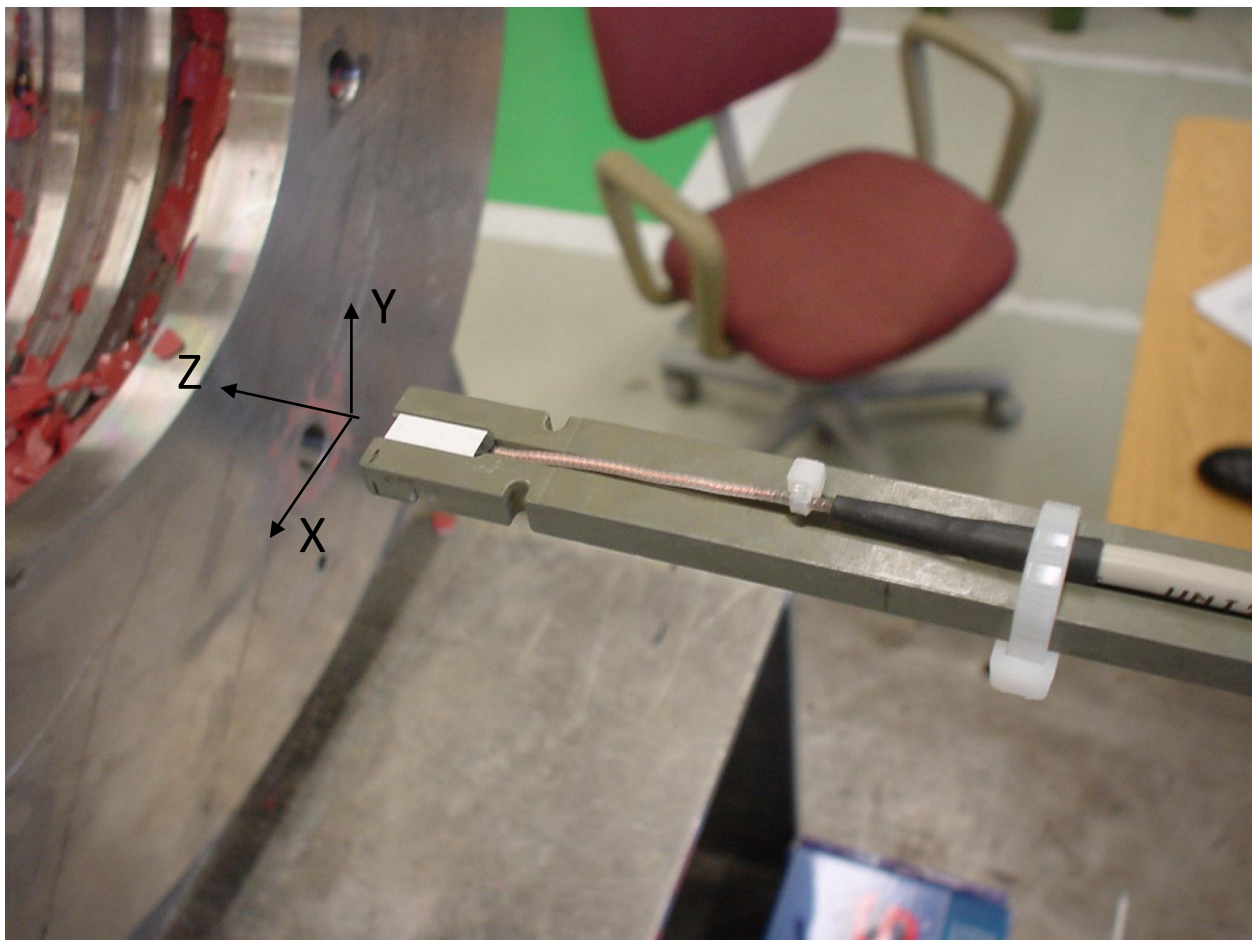

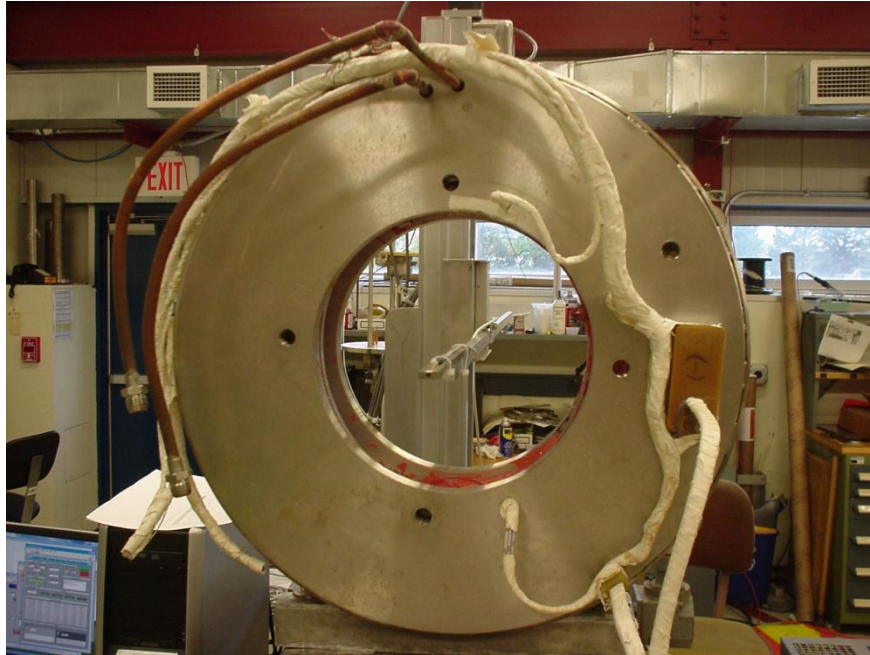Fig. V-3. 3D Senis Hall probe measurement coordinate system coincides with motion coordinate system.

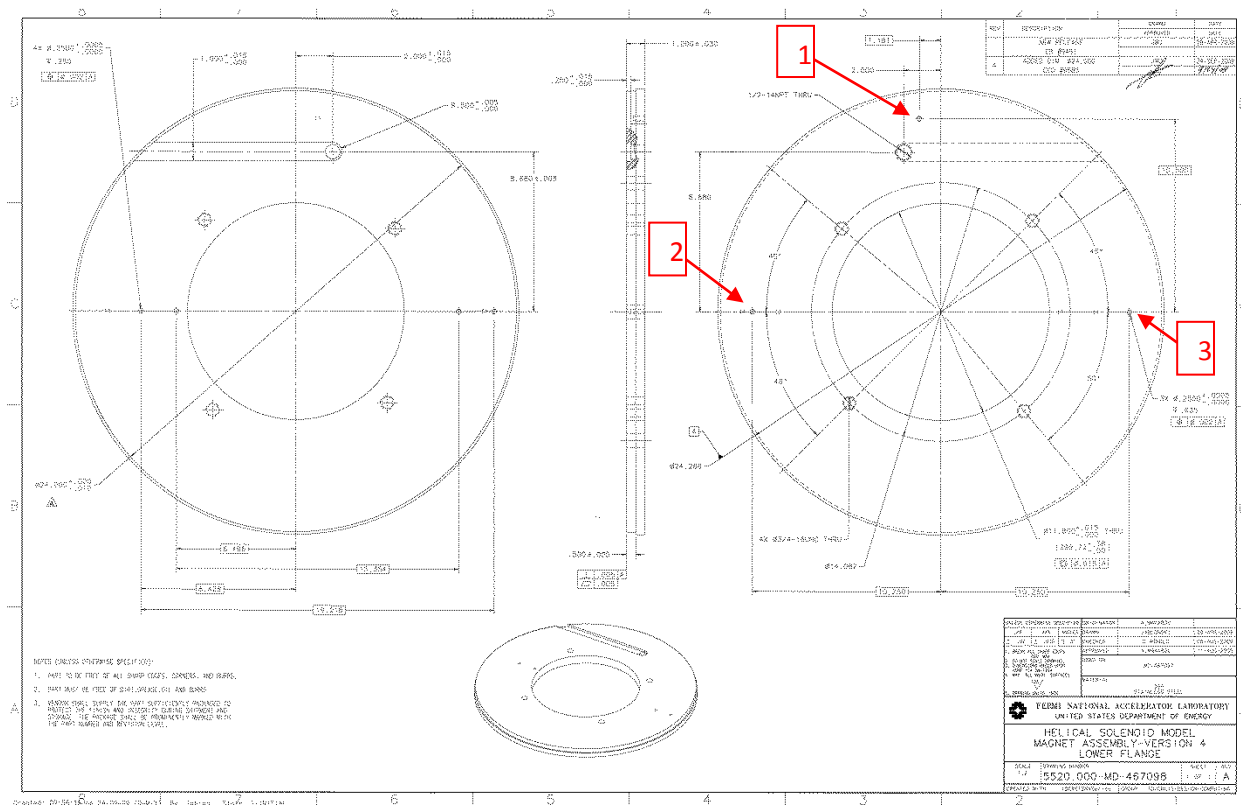Fig. V-4. Lead end of HSM02 showing probe centered in aperture.

Fig. V-5. Subassembly drawing 467098 showing the non-lead end surface and locations of survey fiducial installation holes.

Fig. V-5 shows drawing 467098, which shows the non-lead (RE=Return End) end plate details. Holes for survey targets are indicated (highlighted by red pointers). Compare this to Fig. V-1, and note that the magnet base is mounted so that point 1 is down; point 2 is toward negative X and point 3 is toward positive X direction. The magnet base rests on an aluminum beam which is 12 inches high, above a (magnetic) steel table. Also shown in Fig. V-1, points 2 and 3 are rotated slightly from the (horizontal) X motion axis. Points 2 and 3 are separated by 21.5 inches, and are each 3/8" (9.5 mm) away from the horizontal. On the Lead End (LE), the SC Leads are on the positive X side, at Y<0 (see Fig. V-4).

Comparison of the measurements to a magnetic model have not yet been performed; these are pending survey data to correctly align the 3D model with the measurement coordinate system.

VI. Quench Performance

The quench performance program followed the usual test plan, which starts with training at 4.5 K, continues at lower temperature to study whether limitations are related to mechanical or conductor performance, and explores sensitivity to ramp rates (usually at multiple temperatures). The expected short sample limit and load lines for the coils are shown in Fig. VI-1. The quench current at 4.6 K is predicted to be about 15 kA. The quench training history is shown in Fig. VI-2, also illustrating the magnet temperature history. In this test, initial training was steady but very slow, so temperature was reduced in an attempt to increase the rate of improvement. Following low temperature training (3.0 K), several 4.5 K quenches were made to examine if the highest quench current (14862 A) is maintained, which it was although the magnet exhibited 500-1000 A fall-backs at both temperatures. The first cold test cycle (TC1) ended with a study of the heater efficiency to quench each coil, the magnet was then warmed to room temperature. Intermediate between two helium cold test cycles was a thermal test of conduction cooling to liquid nitrogen temperature, and back to room temperature. A second liquid helium cold test cycle (TC2) was then performed, to study the re-training behavior of coils with this design. As shown in Fig. VI-2, re-training at 4.6 K was relatively fast, and the magnet reached a maximum current of 14884 A.

Fig. VI-3 compares the training histories of HSM01 and HSM02. They are clearly very similar in terms of rate of training and plateau current. However, the expected maximum predicted currents differ by about 8% (~15000 A for HSM02, and ~16500 A for HSM01), so the second model reached a higher percentage of the expected maximum (although the graph suggests that additional training, especially at low temperature, could eventually have yielded a higher value for HSM01).

The history of quenches sorted by location is shown in Fig. VI-4. A summary table of all quenches is appended as Appendix A, and the quench start locations for both HSM02 and HSM01 are summarized in the frequency plot of Fig. VI-5: clearly most quenches originate in the end coils (which is also the peak field region, from Fig. VI-1.), especially in coil 4 (the lead end). Quench development in HSM02 was most likely to be in a single coil, but propagation to adjacent coils was seen in a few cases: either coils A and B, or coils D and C. Note that two quenches (4, 66) started simultaneously in coils C and D. The quench development times are pretty well correlated with the quench current, as shown in Fig. VI-6. Essentially all of the quenches were detected by the half-coil difference AQD at a 400 mV threshold, so a 10 ms quench development implies an average voltage growth of 40 mV/ms (some quenches showed slope change in dV/dt). Two example quench development voltage traces are shown in Fig. VI-7, for ramp 20 which started in coil D then propagated to coil C, and ramp 54 which started first in coil B then in coil A (one of only two coil B quenches). Note that the signals shown here have been filtered to reduce noise.

As with HSM01, the ramp rate dependence (shown in Fig. VI-8) was found to be almost negligible, even out to 300 A/s, and very slight out to 600 A/s. This was measured at 4.6 K just before lower temperature training, and again at the end of TC2. The slightly erratic quench plateau means that one cannot discern the small ramp rate dependence from a training fall-back. Thus it was not worth pursuing this study further after training to the highest current.
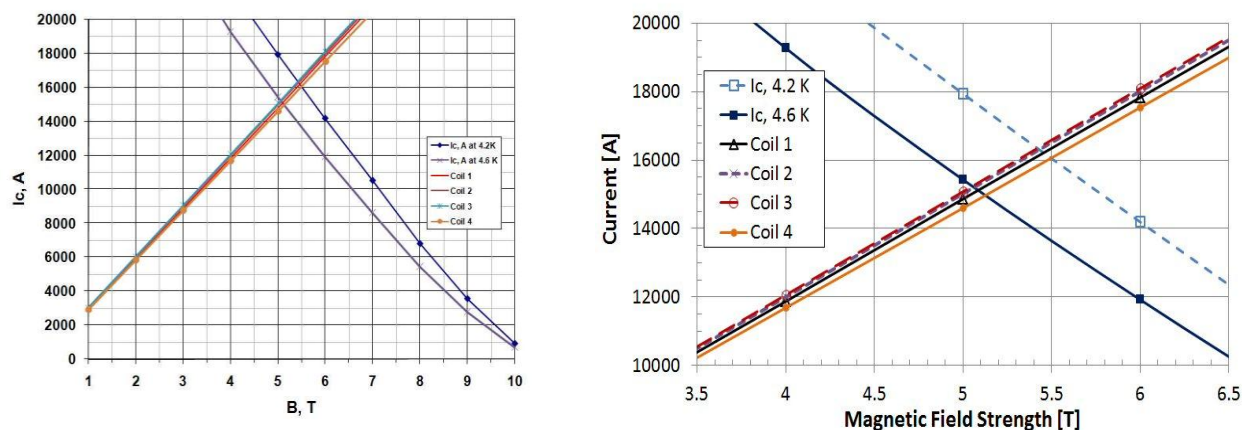
Fig. VI-1. Quench prediction (load lines crossing short sample curves) for HSM02 coils.
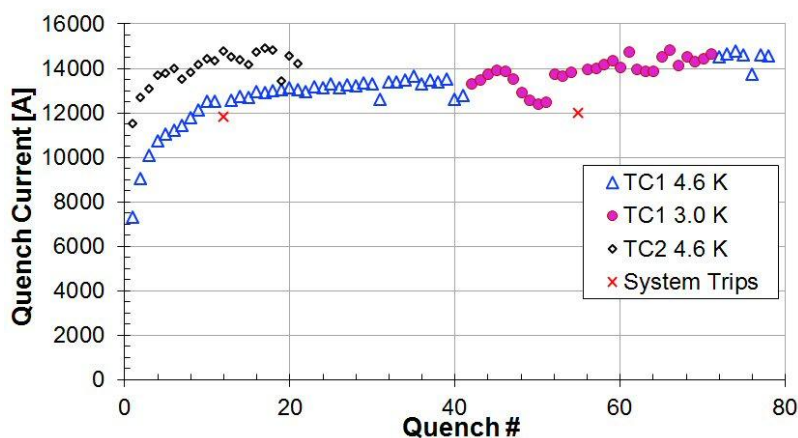
Fig. VI-2. Overlay of quench training history for HSM02 in first and second thermal cycles.
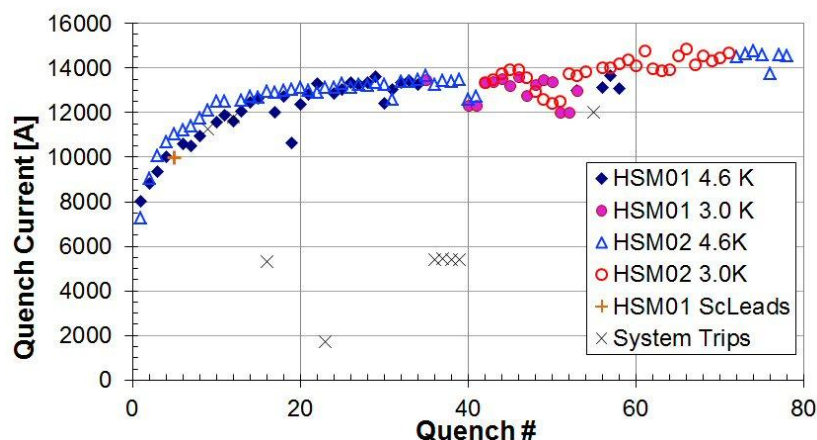
Fig. VI-3. Overlay of quench training history in first thermal cycles for HSM01 and HSM02.
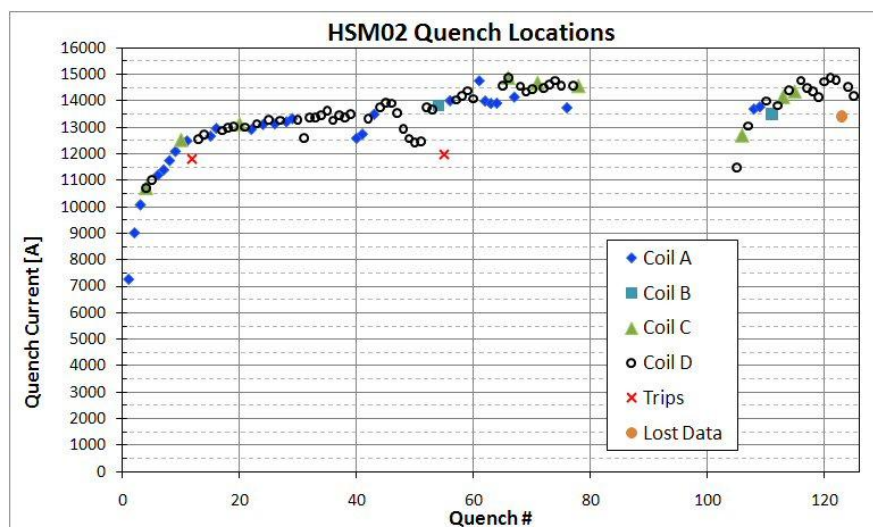
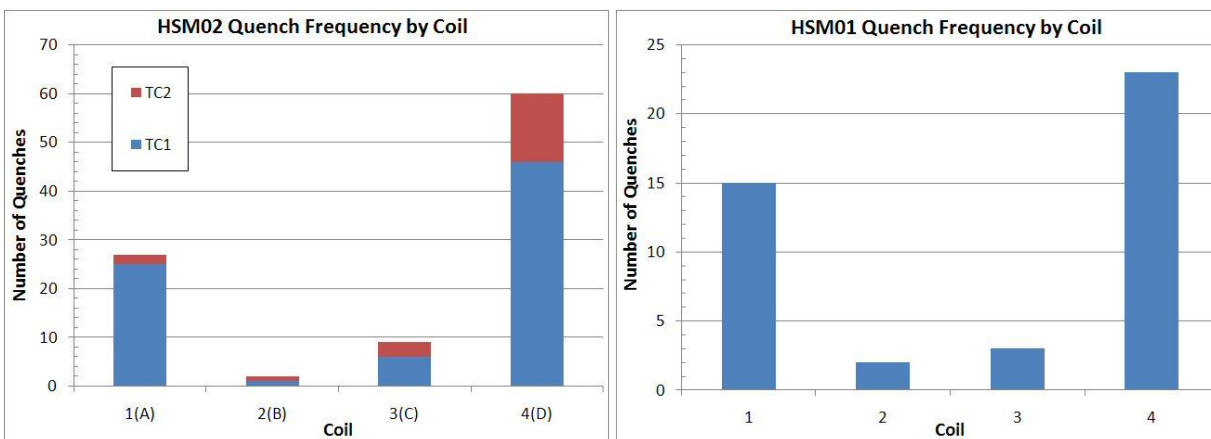Fig. VI-4. Quench history for HSM02, labeled by location, in first thermal cycle.

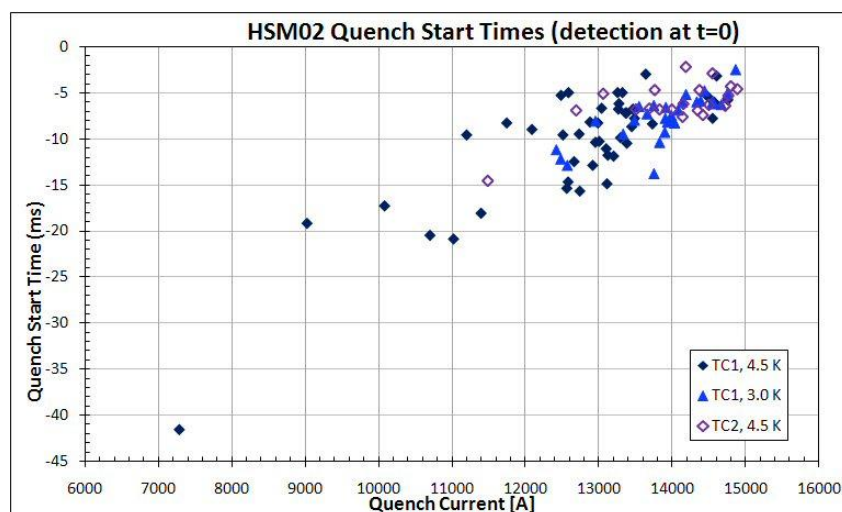Fig. VI-5. Frequency histogram of quench locations for HSM02 (left) and HSM01 (right).

Fig. VI-6. Quench development times as a function of quench current, labeled by helium temperature.
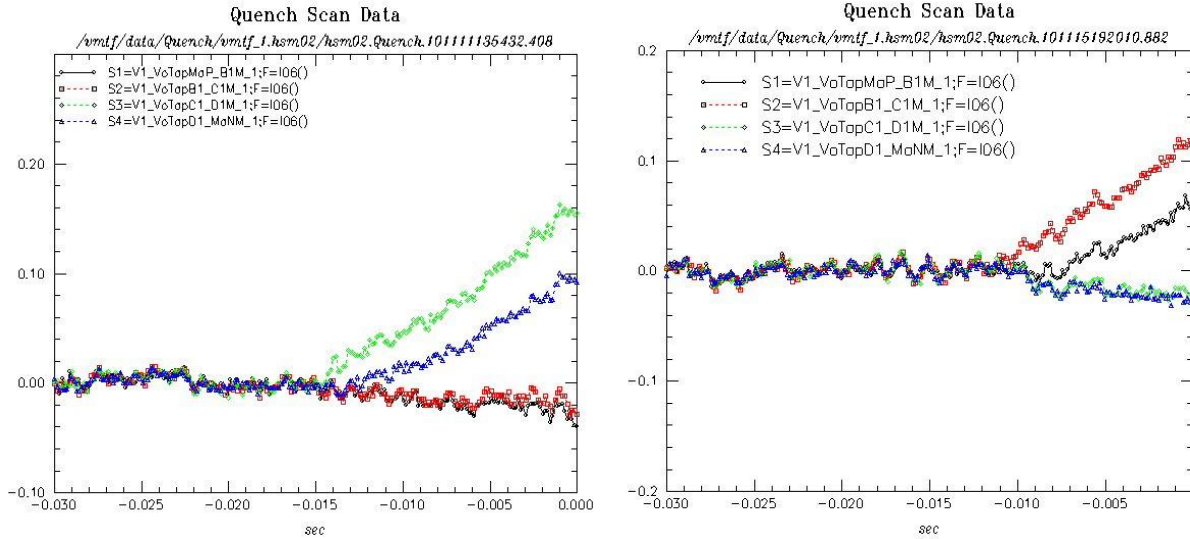
Fig. VI-7. Configurable voltage tap signals for quenching coils in ramp 20 (left) and ramp 54 (right).
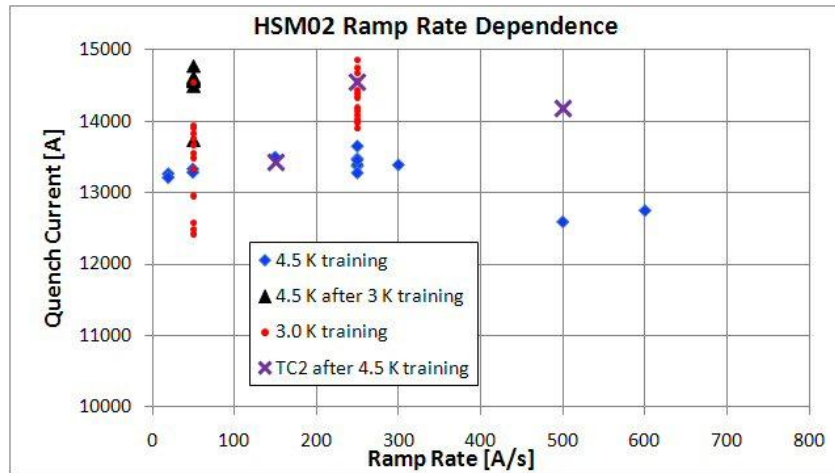

Fig. VI-8. Ramp rate dependence of HSM02 quench current before, during, and after 3 K training.

VII. Spike Data Analysis

The voltage spike detection system (VSDS) based on a National Instruments PXI multifunction DAQ was used for study of thermo-magnetic instabilities in HSM02. The VSDS captures half-coil signals at a sampling rate of 100 kHz. More details on this system are presented in [3]-[4]. The half coil difference signal had a relatively low noise level, about 5-6 mV from peak to peak, with spike detection threshold typically set to 40 mV.

Voltage spike data were captured for most ramps during quench performance studies. Almost no voltage spikes were detected during the magnet training or ramp rate dependence study which could be associated with conductor thermo-magnetic instabilities. Low amplitude (8-12 mV) and narrow spikes at high currents (9-12 kA) could be related to the power supply noise (see Fig. VII-1).
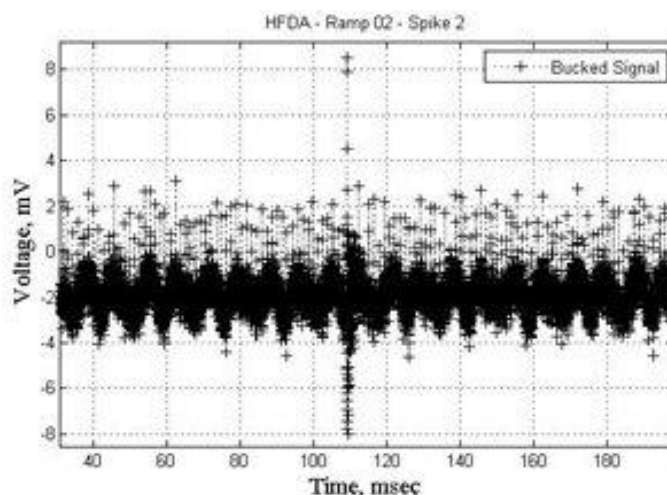
Fig. VII-1. Bucked half-coil signal from the VSDS, triggered by a very short spike at low threshold.

VIII. Protection Heater Studies

A strip heater for quench protection was insulated and installed around the inner mandrel of each coil prior to winding the coils. The protection heaters consisted of ½-inch wide x 5-mil thick copper-clad stainless steel strips encapsulated in 1-mil thick Kapton® insulation, the same material used in HSM01 [2]. The effectiveness of the heaters to induce a quench was studied after the quench training program was completed, by firing individual heaters at a variety of magnet currents. The strip heaters were put in parallel with an external 4 Ω resistor to allow greater range of energy deposition (given the heater firing unit voltage setting limitations). The HFU capacitance was set to the minimum value, 4.8 mF, for all of the tests. Fig. VIII-1 shows the measured delay between the heater firing time and quench detection for the matrix of currents and voltages studied. It appears that coils A and B have very similar effectiveness, while coils C and D are somewhat more efficient at inducing a quench for the same settings. Calculation of the heater power density for these V,C settings has not yet been completed.
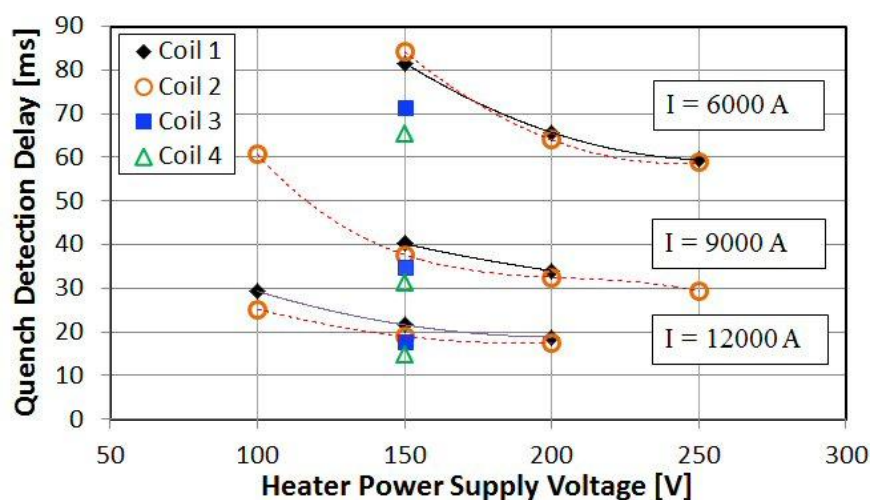

Fig. VIII-1. Delay from heater excitation to quench detection as a function of coil current and heater voltage at 4.6 K. All tests used heater firing unit with 4.8 mF capacitance.

IX. RRR

      Voltage data were captured by the usual method to determine RRR of each coil. The Kepko trim power supply was connected across the magnet and constant current of 4 to 5 A was used to excite the coil with polarity alternating every few minutes. Isoamp gains were set to the "RRR" mode to boost the small signals for good resolution. Data were taken with the magnet at 300 K on 11/05. Cold data were taken on 11/22; the transition to resistive occurred from 18:45 to 18:53 at a temperature of about 9.25 K. The resulting RRR values are shown in Table 2. NOTE: As shown in Fig. IX-1, voltage tap segments made the transition to a resistive state in the opposite order from that expected (coil D first, then C, B, and A). The temperature data are clearly correct – the temperature gradient is warmer at the top (coil A), cooler at the bottom (coil D). Therefore we conclude that the labeling of coils in the quench study is inverted – "Coil A" voltage taps actually refer to the bottom coil, while "Coil D" voltage taps refer to the top coil.

Table 2. RRR values for HSM02 coils

Coil A	Coil B	Coil C	Coil D
102.7	101.0	101.7	102.4

Note that these values are somewhat lower than those measured in HSM01, which had RRR ~145 and was made using the same superconductor cable. This is probably due to the HSM02 cable having been reworked (flattened after annealing) to remove the keystone angle.
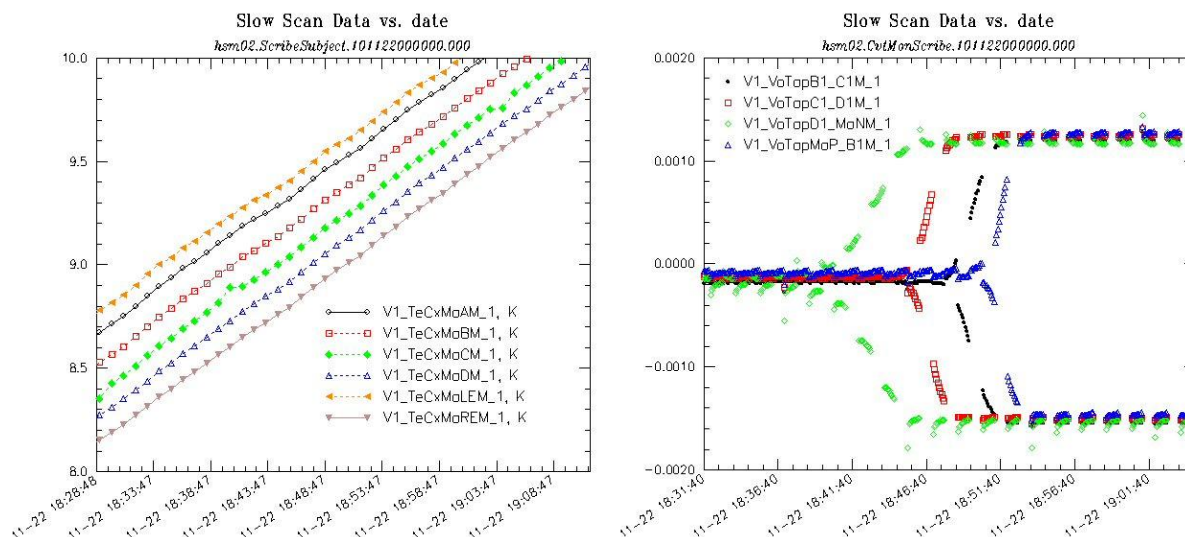

Fig. IX-1. Coil temperatures (left) and coil voltages at ±4.8 A during coil transitions to resistive state.

X. Conduction Cooling Study

      Fig. X-1 shows photographs of the copper cooling tubes that wrap around each coil of HSM02, their connections to the VMTF nitrogen supply and return lines, and the approximate positions of temperature sensors. The magnet reached a temperature of 290 K on November 30 after the first cold test cycle. Starting at 09:30, the VMTF helium vessel was pumped down to a pressure of about 0.15 psia and held at that vacuum level through the cooling test (which improved with time, probably due to cryo-cooling). LN2 was introduced into the cooling tubing, and the coil temperatures began to drop – first coil

D, then coil C, coil B, and finally coil A as shown in Fig. X-2. Tracing LN2 lines shows that the LN2 supply enters and first cools coil D, consistent with data.

There is no temperature sensor to measure the LN2 supply temperature in VMTF; however, the pressure is monitored by a manual gauge which read 47 psig during the test. This translates into a supply temperature of about 92±0.5 K. Unfortunately, the calibrations for both Cernox and Carbon Glass RTDs that measure magnet and dewar temperatures are poor in the range from 80 K to 300 K: {temperature, resistance} points exist only at 78, 200, and 295 K. Thus, the conversions to temperature (by various algorithms, e.g., Chebychev polynomial fit, or local quadratic interpolation) give somewhat imprecise temperatures in the range we are interested in, at the level of about 5 K. These are shown in Fig. X-3, along with the RTD resistance values, which behave in a smooth manner with time; a slight LN2 flow reduction was made at 08:30 on 12/01 that resulted in all temperatures dropping slightly by the same amount (Fig. X-4). Fitting this response to an exponential decay results in a thermal time constant of about 2500 seconds at 92 K. Better calibrations could be applied offline to get more precise temperature profiles. Comparison with a thermal model is left as an exercise for the future.

The LN2 conduction cooling test continued on 12/01, with temperatures remaining steady, until 14:50, at which time the LN2 flow was turned off and warm up began. The dewar pressure was raised at 15:10 to accelerate the magnet warm up to room temperature.
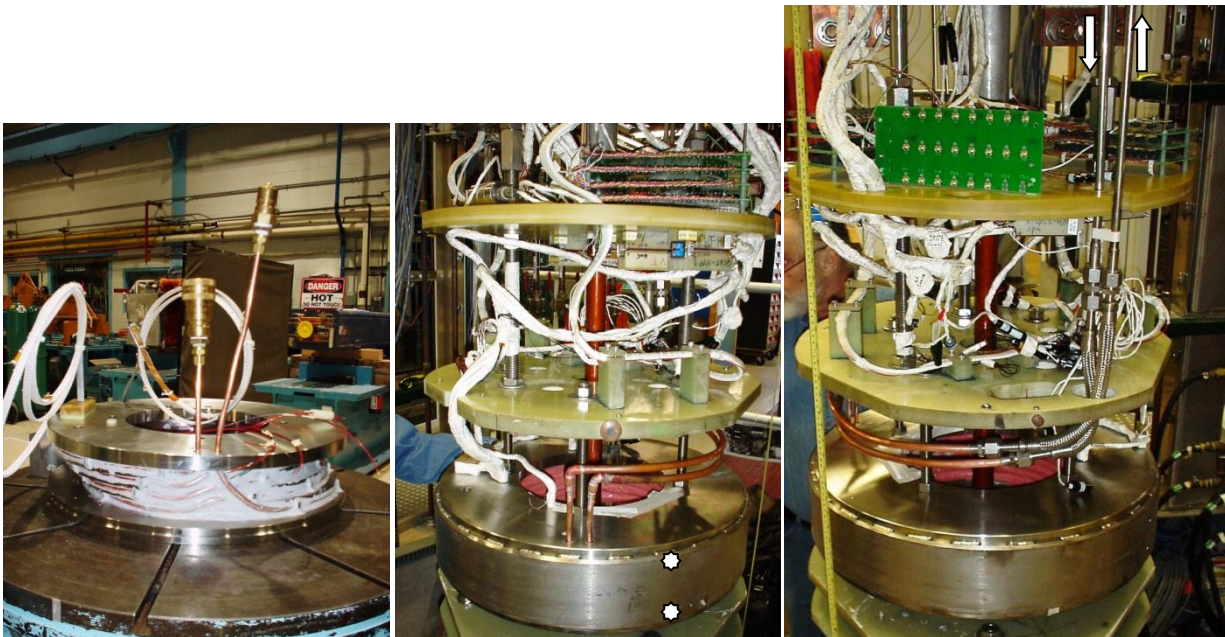

Fig. X-1. Copper cooling tubes for conduction cooling of HSM02 coils, and their connections to the VMTF supply and return pipes (arrows). Top and Bottom RTD locations on the outer skin are shown (white spots) in the center picture; those on the rings are on the inner circumference in the same region (see Fig. III-1).
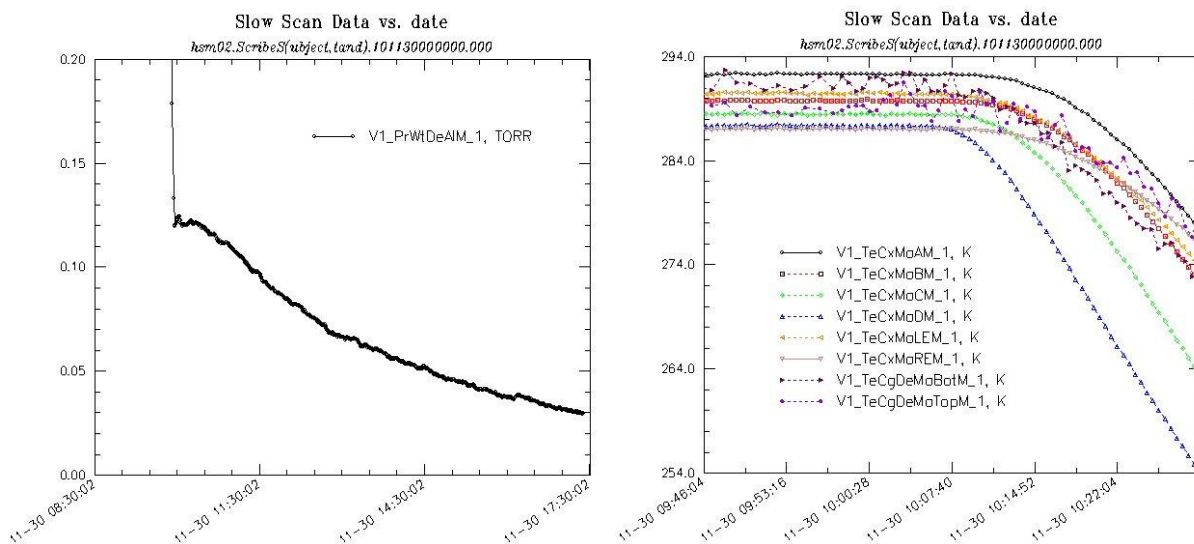
Fig. X-2. Conduction cooling test showing VMTF pressure (left) and magnet skin temperatures (right) at start of the test.
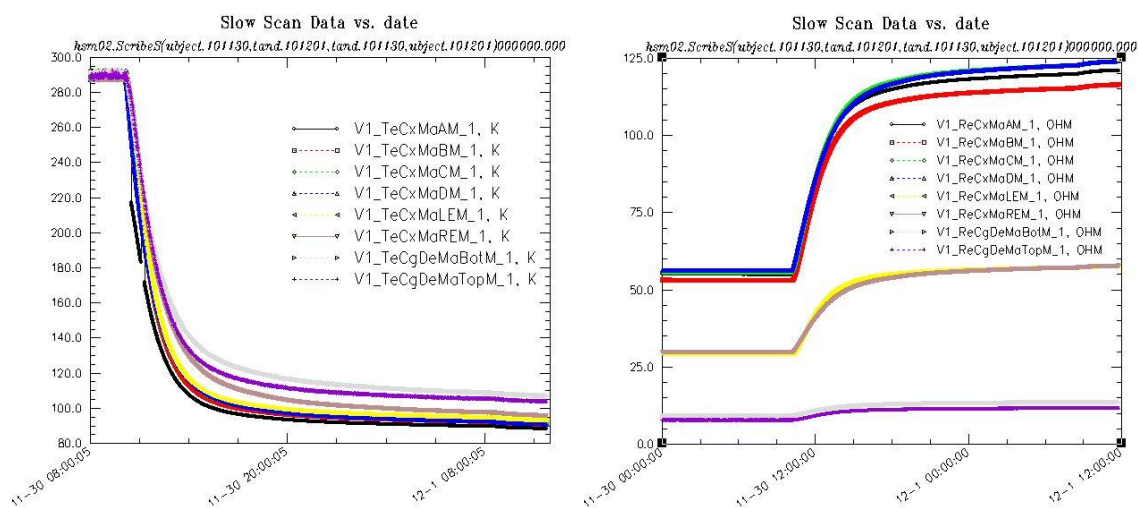

Fig. X-3. Conduction cooling test temperatures (left) and RTD resistances (right).
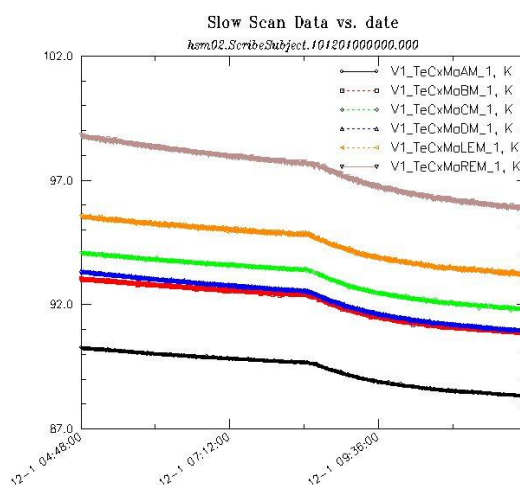

Fig. X-4. Response of coil and end plate temperature sensors following slight LN2 flow reduction.

The HSM02 assembly was removed from VMTF on January 3, 2011. Upon inspection, it was obvious that something unexpected had occurred to the copper tubing used for the LN2 conduction test: Fig. X-5 shows photos of the copper tubing after the removal, which indicate they were subjected to electrical arcs and large forces that displaced the tubes from their original orientation (compare with Figs. X-1). An electrical checkout found no anomalies with the NbTi coil – in particular, there were no hipot failures to ground or the copper tubing. The conclusion is that this damage must be the result of the tubing acting as a (40 turns: 4 turns) 10:1 step-down transformer with the solenoid coils. The highest current in the copper tubing would result when the 30 mΩ energy extraction dump is fired following a quench: at 15kA (the highest current) the voltage across the coil would be 900 V, and therefore 90 V would be induced across the tubing "circuit" – a loop which may be completed where the stainless inlet and outlet connections were made (and where evidence of arcing also was found). An estimate of the current in the copper tubing, assuming the room temperature copper resistance of 3.2 mΩ, gives I> 28 kA; being in a large ~1 T fringe field of the solenoid, even a 1 kA current results in a Lorentz force on the tubing of 1 kN/m which can easily bend the tubing. The clear lesson from this outcome is that the arrangement of tubing for conduction cooling must be designed to avoid net magnetic coupling with the main coils.
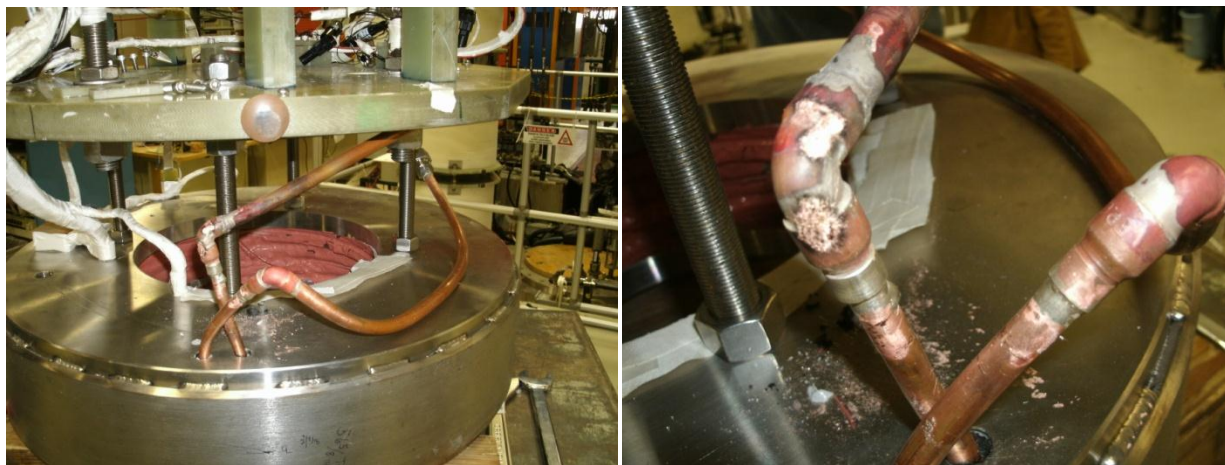

Fig. X-5. Photos of distorted and sputtered copper tubing after HSM02 cold test.

XI. Strain Gauges

Fig. XI-1 shows the temperatures at which strain gauge cool down and warm up values are to be found (300 K and 4.6 K periods). The strain gauge voltages are shown in Fig. XI-2, which indicate two main features: two gauges had large shifts during the cool down (compensator, and coil B), and did not return to their room temperature values after warm up – suggesting that they may have come de-bonded from their surfaces. Of the others, the room temperature values are close but slightly below the original warm values, except for coil B which returned to the same value. The dependence on squared magnet current is shown in Fig. XI-3 during the initial training on 11/12, and again after the thermal cycle on 12/09: all of the gauges show a linear response, but the slopes vary. It is surprising that the coil B gauge (which may have de-bonded) has a greater slope than the compensator (which should reflect the magneto-resistance effect), while the coil A gauge matches the compensator; the gauge cold offsets have been shifted to align all of the voltages at 0 A.
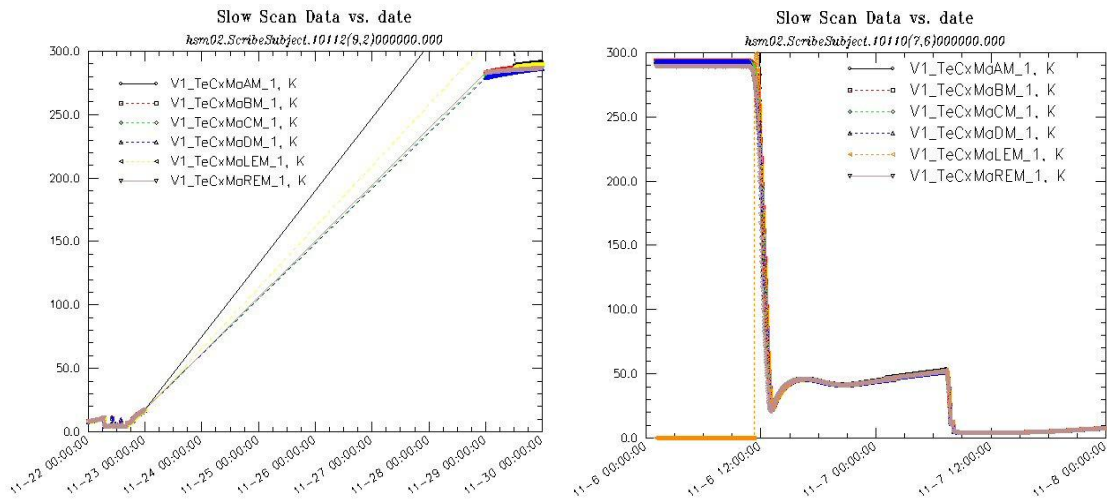
Fig. XI-1. Temperatures before and after warm up (left) and during initial cool down (right).
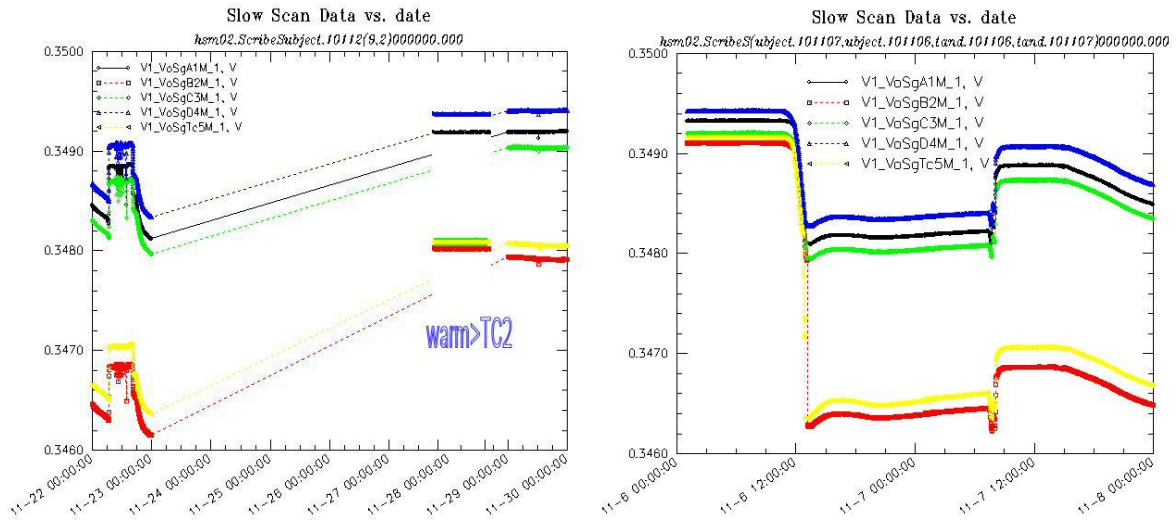

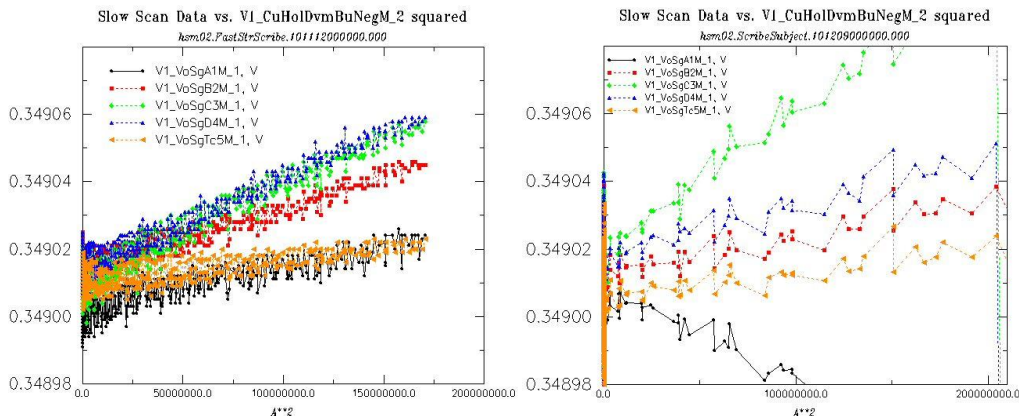Fig. XI-2. Strain gauge voltages before and after warm up(left) and during first cool down (right).

Fig. XI-3. Strain gauge voltages plotted as a function of squared current, at 4.6 K on 11/12 (left, including ramp rate studies), and during re-training on 12/09 after a thermal cycle (right).

XII. Conclusions

A second 4-coil helical solenoid HSM02 with NbTi conductor was built and tested. Several design changes were made based on the experience of HSM01 which improved performance in the second model. Quench training of the epoxy-impregnated coils was slow, but the rate of training was nearly the same for both and they achieved quench plateau currents at 85 % and 100 % of the expected maximum. For both, most quenches occurred in the end coils, so one may anticipate that in longer HS magnets the training rate will not scale quickly with the number of coils. Ramp rate dependence is negligible, and re-training after a thermal cycle is fast. Magnetic field measurements agree well with model predictions, and efforts continue on improving coordinate systems to relate these. Although the second model had provisions for a conduction cooling study, a proper facility to perform the test does not yet exist. However, the attempted study provided information to improve cooling loop design and make better temperature measurements.

References
1. M. Zisman, "The Muon Collider,"
   http://www.osti.gov/energycitations/product.biblio.jsp?osti_id=1004168
2. S. A. Kahn, et al, "Magnet System for Helical Muon Cooling Channels", MOPAN117, Proceedings of PAC'07.
3. V. S. Kashikhin, et al, "Superconducting Magnet System for Muon Beam Cooling," *IEEE Trans. Appl. Supercon.*, Vol. 17, No. 2, pp. 1055-1058, June 2007.
4. K. Yonehara, et al., "The MANX Muon Cooling Demonstration Experiment", THPMN110, Proceedings of PAC'07.
5. V. S. Kashikhin, et al, "Magnets for the MANX 6D Muon Cooling Demonstration Experiment," MOPAS012, Proceedings of PAC'07.
6. V. S. Kashikhin, "Four-coil superconducting helical solenoid model for muon beam cooling," WEPD013, Proceedings of EPAC'08.
7. M. Tartaglia, et al., "Test of four coil helical solenoid magnet HSM01," FNAL, TD-09-011, April 2009.
8. B. Bordini et al., "Voltage spikes in Nb_3Sn and NbTi Strands", IEEE Trans. Appl. Superconduct., Vol. 16, Issue 2, June 2006, pp 366-369
9. D.F. Orris et al., "Voltage Spike Detection in High Field Superconducting Accelerator Magnets," IEEE trans. Appl. Superconduct., Vol. 15, Issue 2, June 2005, pp 1205-1208

Appendix A. Table of quench events

\\tdserver1\ic\Run Support\VMTF\LIST_of_MAGNETS\MuCool_HSM02\QuenchSummary\HSM02_QH_1122.xlsx